Journal of Solid State Chemistry 183 (2010) 2121–2126

Contents lists available at ScienceDirect

Journal of Solid State Chemistry

journal homepage: www.elsevier.com/locate/jssc

Crystal structure and physical properties of the new ternary antimonides $Ln_3Pd_8Sb_4$ (Ln=Y, Gd, Tb, Dy, Ho, Er, Tm)

Mariya Zelinska [a,b], Stepan Oryshchyn [a], Olga Zhak [a], Jean-Yves Pivan [b], Michel Potel [b], Olivier Tougait [b], Henri Noel [b], Dariusz Kaczorowski [c,*]

[a] Department of Analytical Chemistry, Ivan Franko National University of Lviv, Kyryla and Mefodija Str. 6, 79005 Lviv, Ukraine
[b] Sciences Chimiques de Rennes, UMR CNRS 6226, Université de Rennes 1 – ENSCR, Campus de Beaulieu, Avenue du Général Leclerc, 35042 Rennes Cedex, France
[c] Institute of Low Temperature and Structure Research, Polish Academy of Sciences, P.O. Box 1410, 50-950 Wroclaw, Poland

ARTICLE INFO

Article history:
Received 12 April 2010
Received in revised form
23 June 2010
Accepted 3 July 2010
Available online 11 July 2010

Keywords:
Antimonides
Crystal structure
Magnetic properties
Electrical transport

ABSTRACT

The ternary antimonides $Ln_3Pd_8Sb_4$ (Ln=Y, Gd, Tb, Dy, Ho, Er, Tm) have been synthesized for the first time. The crystal structure of $Er_3Pd_8Sb_4$ has been solved from the X-ray single crystal data: own type structure, space group $Fm\bar{3}m$, a=1.3050(1) nm, R_F=0.0484, R_W=0.0524 for 17 free parameters and 401 reflections with $F(hkl) > 4\sigma(F)$. The structure of $Er_3Pd_8Sb_4$ can be viewed as a ternary ordered version of the $Sc_{11}Ir_4$-type. The lattice parameters of the isotypic compounds $Ln_3Pd_8Sb_4$ (Ln=Y, Gd, Tb, Dy, Ho, Tm) have been refined from the X-ray powder diffraction data. The magnetic and electrical properties of the compounds $Ln_3Pd_8Sb_4$ (Ln=Tb, Ho, Er) have been studied down to 1.75 K. The Ho- and Er-based phases have been found to order antiferromagnetically at 2.5 and 2.0 K, respectively. For all three compounds, the magnetic susceptibility follows in the paramagnetic region the Curie–Weiss behavior with the effective magnetic moments close to the respective free trivalent ion values. All three antimonides studied exhibit metallic character of the electrical conductivity.

1. Introduction

Rare-earth-antimony-based compounds have attracted considerable attention because of great variety in their crystal-chemistry behaviors and their remarkable physical properties. These systems possess very rich phase diagrams with several intermediate phases that exhibit interesting structural features, such as original types of crystal structures, formation of superstructures, low-dimensional character of atom arrangement. With respect to the electronic properties, they display wide range of magnetic phenomena ranging from well localized paramagnetism to spin-glass-like or long-range magnetic order, while their electrical transport properties vary from narrow-band semiconducting to metallic behavior. Some ternary antimonides are being considered as potential materials for modern thermoelectric devices.

To the best of our knowledge, the phase-relations in the ternary Ln–Pd–Sb systems were not studied systematically, and only crystallographic data and some physical properties are known for few intermediate compounds [1]. In the Er–Pd–Sb system, only three ternary antimonides were known, namely ErPdSb (MgAgAs-type structure) [2,3], $ErPd_2Sb$ ($MnCu_2Al$-type structure) [4,5] and Er_5Pd_2Sb (Mo_5B_2Si-type structure) [6], making this system of interest for the discovery of additional phases. The new compound $Er_3Pd_8Sb_4$ was isolated in the course of our systematic investigation of the ternary Er–Pd–Sb system. It crystallizes with a crystal structure of its own type, which may be described as a ternary version of the $Sc_{11}Ir_4$-type [7], and which shows close relationships to the Th_6Mn_{23} [8] and $Mg_6Cu_{16}Si_7$-types [9]. Numerous compounds adopting the filled Th_6Mn_{23}-type structure have been reported in the literature [10]. Among them are the binary intermetallics $Sc_{11}Os_4$, and $Zr_{11}Os_4$ [7], as well as the ternary phases $Zr_6Zn_{23}Si$ [11], $U_6Fe_{16}Si_7C$ [12], and the so-called G phases [13].

In this paper, we report on the formation of the compounds $Ln_3Pd_8Sb_4$ (Ln=Y, Gd, Tb, Dy, Ho, Er, Tm), the refinement of the crystal structure performed for $Er_3Pd_8Sb_4$, as well as on the magnetic and electrical properties of $Tb_3Pd_8Sb_4$, $Ho_3Pd_8Sb_4$ and $Er_3Pd_8Sb_4$.

2. Experimental

2.1. Synthesis

Polycrystalline samples of the compounds $Ln_3Pd_8Sb_4$ (Ln=Y, Gd, Tb, Dy, Ho, Er, Tm) were prepared by melting elements (all

* Corresponding author. Fax: +48 71 34 410 29.
E-mail address: D.Kaczorowski@int.pan.wroc.pl (D. Kaczorowski).

0022-4596/$ - see front matter © 2010 Elsevier Inc. All rights reserved.
doi:10.1016/j.jssc.2010.07.002

with the stated purity better than 99.9 wt%) in an arc-furnace under purified argon atmosphere. The buttons were flipped over and remelted two times to achieve homogeneity. Because of high vapor pressure of antimony, an excess of 2 at% of Sb was added to the starting mixture. Subsequently, the samples were placed in alumina crucibles and sealed in fused silica tubes under primary vacuum. They were then heat-treated at 700 °C for a period ranging from 240 to 360 h.

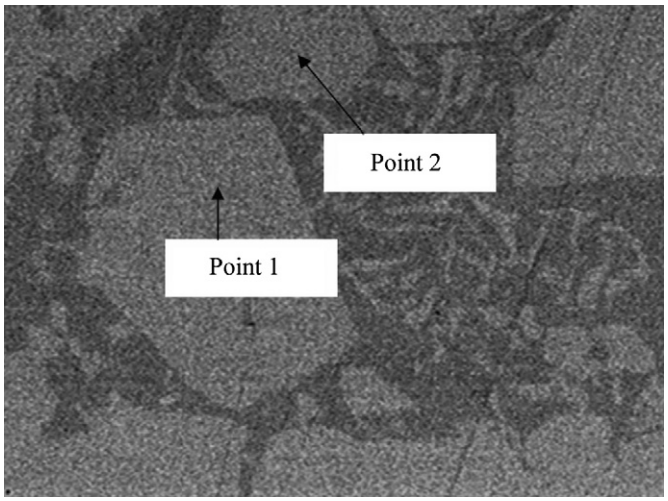

Fig. 1. Backscattered image of a microsection of the sample Er:Pd:Sb of 15:45:40, showing large grains of $Er_3Pd_8Sb_4$ revealed as light gray color.

2.2. Powder X-ray diffraction

A small part of each sample was pulverized and analyzed by X-ray diffraction (XRD) using a powder diffractometer (CPS 120 INEL) equipped with a position-sensitive detector (ranging from 6° to 120° in 2θ) using Cu$K\alpha_1$-radiation. Comparison of the obtained diffraction patterns with those corresponding to various structure-types was carried out with help of the program POWDERCELL [14].

2.3. Crystal structure determination

The intensity data were collected at ambient temperature, with the help of a Bruker Kappa CCD diffractometer, using the Mo$K\alpha$ radiation (λ=0.071073 nm). The unit-cell parameters, orientation matrix as well as the crystal quality were derived from 10 frames recorded at χ=0 using a scan of 1° in φ. The complete strategy to fill more than a hemisphere was automatically calculated with the use of the program COLLECT [15]. Data reduction and reflection indexing were performed with the program DENZO of Kappa CCD software package [15]. The scaling and merging of redundant measurements of the different data sets as well as the cell refinement was performed using DENZO. Semi-empirical absorption corrections were made with the use of the program MULTISCAN [16]. Structure models were determined by direct methods using SIR-97 [17]. All the structure refinements and the Fourier syntheses were made with the help of the CSD software [18]. The atomic positions were standardized with the help of STRUCTURE TIDY [19]. The representations of the crystal structures were drawn with the help of DIAMOND 2.1 [20].

Table 1
Crystallographic and structure refinement data for $Er_3Pd_8Sb_4$.

Structure type	Own
Space group	$Fm\bar{3}m$
Lattice parameters	
a, (nm)	1.3050(1)
V (nm^3)	2.2224(5)
Formula units, Z	8
Calculated density (g/cm^3)	10.997(3)
Absorption coefficient (cm^{-1})	450.78
Diffractometer	Nonius Kappa CCD
Radiation and wavelength (nm)	Mo$K\alpha$ (λ=0.071073)
$2\theta_{max}$ (deg); $(\sin\theta/\lambda)_{max}$	79.90; 0.903
Collected reflections	11 703
Unique reflections	400
Conditions of refinement	F (hkl), $F(hkl) > 4\sigma F(hkl)$
Unique reflections used in refinement	331
Variable parameters	17
R_F; wR_F	0.0484; 0.0524
Largest diff. peak and hole (e^-/Å^{-3})	3.62/−3.17

Table 3
The interatomic distances (δ) and the coordination numbers (CN) of the atoms in $Er_3Pd_8Sb_4$.

Atoms		δ (Å)	CN	Atoms		δ (Å)	CN
Er1	1Sb2	2.925(1)	14	Pd2	3Sb1	2.664(1)	12
	4Pd1	3.002(1)			3Pd1	2.938(2)	
	4Pd2	3.160(1)			3Pd2	3.090(2)	
	2Sb1	3.2800(2)			3Er1	3.160(1)	
	2Sb1	3.2800(1)		Sb1	4Pd2	2.664(1)	12
	1Sb3	3.600(1)			4Pd1	2.875(1)	
Pd1	1Sb3	2.686(1)	13		4Er1	3.2800(2)	
	3Sb1	2.875(1)		Sb2	6Er1	2.925(1)	6
	3Pd2	2.938(2)		Sb3	8Pd1d1	2.686(1)	14
	3Er1	3.002(1)			6Er1	3.600(1)	
	3Pd1	3.101(2)					

Table 2
The atomic coordinates[a] and the displacement parameters (in Å^2) in $Er_3Pd_8Sb_4$.

Atom	Wyckoff position	x/a	y/b	z/c	U_{eq}[b]	U_{11}	U_{22}	U_{33}	U_{12}	U_{13}	U_{23}
Er1	24e	0.2759(1)	0	0	0.0117(2)	0.0097(3)	U_{11}	0.0156(5)	0	0	0
Pd1	32f	0.11883(8)	x	x	0.0120(2)	0.0120(3)	U_{11}	U_{11}	−0.0017(3)	U_{12}	U_{12}
Pd2	32f	0.33371(9)	x	x	0.0125(2)	0.0125(2)	U_{11}	U_{11}	0.0025(4)	$-U_{12}$	$-U_{12}$
Sb1	24d	0	1/4	1/4	0.0090(3)	0.0076(6)	0.0097(4)	U_{22}	0	0	0.0009(5)
Sb2	4b	1/2	1/2	1/2	0.0095(4)	0.0095(7)	U_{11}	U_{11}	0	0	0
Sb3	4a	0	0	0	0.0081(4)	0.0081(6)	U_{11}	U_{11}	0	0	0

[a] The atomic coordinates were standardized using STRUCTURE TIDY program [19].
[b] $U_{eq}=4/3(U_{11}a^{*2}a^2+\cdots+2U_{23}b^*c^*bc\cos\alpha)$.

2.4. Scanning electron microscopy

Scanning electron microscopy and energy-dispersive spectroscopy (SEM–EDS) were performed on pieces of each sample embedded in epoxy resin and polished down to 1 μm, using first SiC paper (down to 10 μm) and then diamond paste. The sample was then coated with thin graphite layer to obtain a good surface conductivity. The compositional contrast among various phases was revealed by means of a backscattered electron detector on a Jeol JSM-6400 scanning electron microscope and chemical analyses were obtained with an Oxford Link Isis energy-dispersive spectrometer.

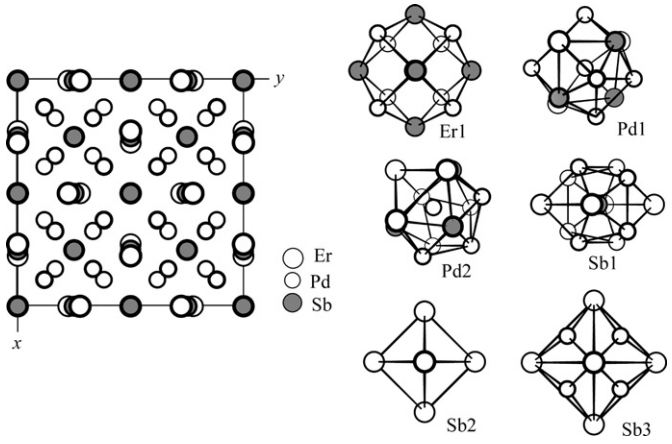

Fig. 2. Projection of the crystal structure of $Er_3Pd_8Sb_4$ onto *xy* plane and the coordination polyhedra of all the atoms.

2.5. Magnetic susceptibility and electrical resistivity measurements

Magnetic measurements were carried out in the temperature range from 1.72 to 300 K and in applied magnetic fields up to 5 T using a Quantum Design SQUID magnetometer. The electrical resistivity was measured in the interval 0.35–300 K employing a standard AC four-probe technique implemented in a Quantum Design PPMS platform. The current leads were attached to the specimens using silver paste, while the voltage contacts were made by spot welding.

3. Results and discussion

3.1. Crystal structure of $Er_3Pd_8Sb_4$

A small single crystal of prismatic form was isolated from the button of the nominal composition Er:Pd:Sb=15:45:40. The SEM photography of the sample is shown in Fig. 1, where well-defined grains of light gray color are clearly visible. The EDS analyses of these area show the presence of erbium, palladium and antimony with an average atomic ratio calculated over 5 points, Er:Pd:Sb of 20(1):53(1):27(1), well matching the crystallographic formula $Er_3Pd_8Sb_4$.

Preliminary single-crystal investigations revealed cubic symmetry of the structure with the lattice parameter $a=1.3050(1)$ nm. Further analysis of systematic reflections appointed the space group $Fm\bar{3}m$. The conditions of crystal structure refinement and the main crystallographic data are gathered in Table 1. The crystal structure of $Er_3Pd_8Sb_4$ was solved by direct methods. The atomic coordinates and the thermal parameters of the atoms are given in Table 2, while the interatomic distances are listed in Table 3.

The crystal structure of $Er_3Pd_8Sb_4$ is characterized by the ordered distribution of Er, Pd and Sb atoms over six

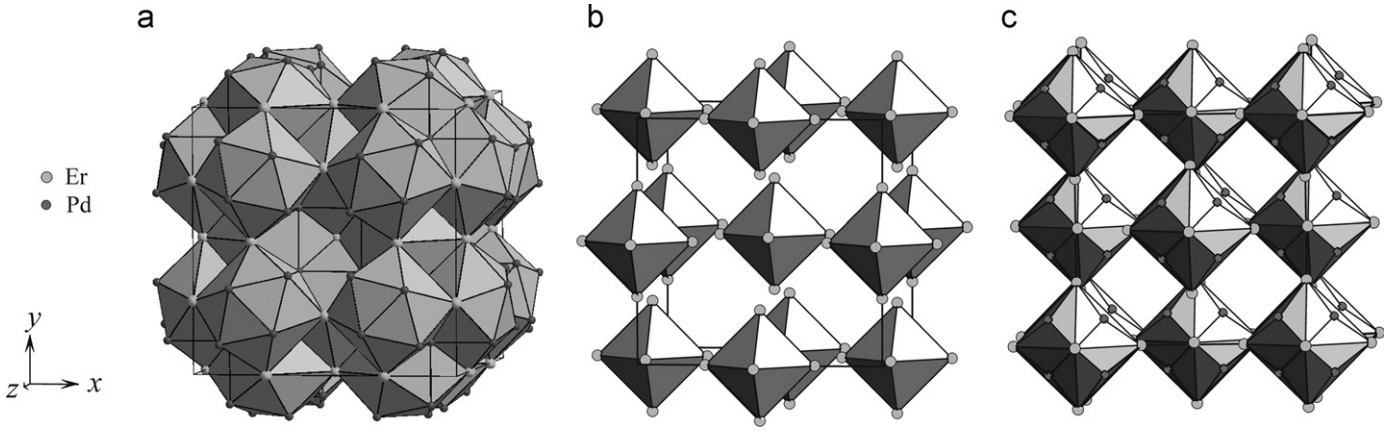

Fig. 3. Arrangement of the coordination polyhedra of the atoms Sb1 (a), Sb2 (b), and Sb3 (c) in the crystal structure of $Er_3Pd_8Sb_4$.

Table 4
Comparison[a] of the Th_6Mn_{23}, $Mg_6Cu_{16}Si_7$, $Sc_{11}Ir_4$ and $Er_3Pd_8Sb_4$ crystal structure types (space group $Fm\bar{3}m$).

Wyckoff position	Atomic coordinates	Th_6Mn_{23}		$Mg_6Cu_{16}Si_7$		$Sc_{11}Ir_4$		$Er_3Pd_8Sb_4$	
		Atom	*x*	Atom	*x*	Atom	*x*	Atom	*x*
32*f*	*x*, *x*, *x*	Mn1	0.122	Cu1	0.1230	Sc1	0.1167	Pd1	0.11883
32*f*	*x*, *x*, *x*	Mn2	0.322	Cu2	0.3316	Sc2	0.3433	Pd2	0.33371
24*e*	*x*, 0, 0	Th	0.297	Mg	0.3176	Sc3	0.3005	Er	0.27590
24*d*	$0, \frac{1}{4}, \frac{1}{4}$	Mn3		Si1		Ir1		Sb1	
4*b*	$\frac{1}{2}, \frac{1}{2}, \frac{1}{2}$	–		–		Ir2		Sb2	
4*a*	0, 0, 0	Mn4		Si2		Ir3		Sb3	

[a] The atomic coordinates in all the structures were standardized using STRUCTURE TIDY program [19]. The coordinates origin is 1/2,1/2,1/2.

crystallographic positions. There is only one inequivalent position for Er, two for Pd, and three for Sb in the unit cell. Projection of the $Er_3Pd_8Sb_4$ unit cell onto *XY* plane is shown in Fig. 2 together with the coordination polyhedra of all the atoms. The Er atom centres a 14-vertices polyhedron, which can be derived from an distorted cube of 8 Pd atoms, with its 6 faces additionally capped by Sb atoms. The coordination sphere of the Pd2 atom is an icosahedron (coordination number CN=12). The Pd1 atom is located inside a 13-vertices polyhedron that is characteristic of the Th_2Ni_{17}-type structure [21]. The coordination polyhedron of the Sb1 atom is a distorted icosahedron formed by eight Pd atoms and four Er atoms. Six Er atoms form a regular octahedron around the Sb2 atom. In turn, the Sb3 atom is in the centre of a cube formed by eight Pd1 atoms, and the next coordination sphere includes also six Er atoms, which are at the vertices of an octahedron. Thus, the entire coordination of Sb3 has the form of an rhombododecahedron (CN=14). The arrangements of the coordination polyhedra of the three antimony atoms in the crystal structure of $Er_3Pd_8Sb_4$ are displayed in Fig. 3.

Table 5
Values of the cubic lattice parameter and the unit cell volume of the compounds $Ln_3Pd_8Sb_4$ (*Ln*=Y, Gd, Tb, Ho, Tm).

Compound	*a* (nm)	*V* (nm^3)
$Y_3Pd_8Sb_4$	1.3075(5)	2.235(3)
$Gd_3Pd_8Sb_4$	1.3114(2)	2.255(1)
$Tb_3Pd_8Sb_4$	1.3140(5)	2.269(3)
$Dy_3Pd_8Sb_4$	1.3087(4)	2.241(2)
$Ho_3Pd_8Sb_4$	1.3078(3)	2.237(2)
$Er_3Pd_8Sb_4$[a]	1.3052(2)	2.223(1)
$Tm_3Pd_8Sb_4$	1.3034(8)	2.214(4)

[a] Lattice parameter refined from X-ray powder data.

From Figs. 2 and 3 one may reveal some interesting combinations of groups of atoms present in the crystal structure of $Er_3Pd_8Sb_4$. Apparently, six Er atoms forming an octahedron around the Sb2 atom, are surrounded by eight Pd2 atoms placed in front of each facet of the octahedron. In turn, in front of the edges of this octahedron there are 12 Sb1 atoms. Furthermore, 24 Pd1 atoms are located in the next coordination sphere in the form of squares opposite to each top of the octahedron. Finally, in front of the squares made by the Pd1 atoms, six Sb3 atoms are placed. The entire group of atoms $[Sb^{(2)}Er_6Pd_8^{(2)}Sb_{12}^{(1)}Pd_{24}^{(1)}Sb_6^{(3)}]$, with an octahedron of Er atoms being in its centre, form layers in the compact cubic packing of the atoms of different size.

The crystal structure of $Er_3Pd_8Sb_4$ can be considered as a ternary version (superstructure of the first order, according to Ref. [22]) of the binary $Sc_{11}Ir_4$-type [7]. The two structure types have the same space group and atom positions: space group $Fm\bar{3}m$, Pearson code *cF*120, TYPIX classification *f2edba*. The $Er_3Pd_8Sb_4$-type structure originates from the $Sc_{11}Ir_4$-type structure upon substituting the Er atoms for the Sc atoms in the crystallographic

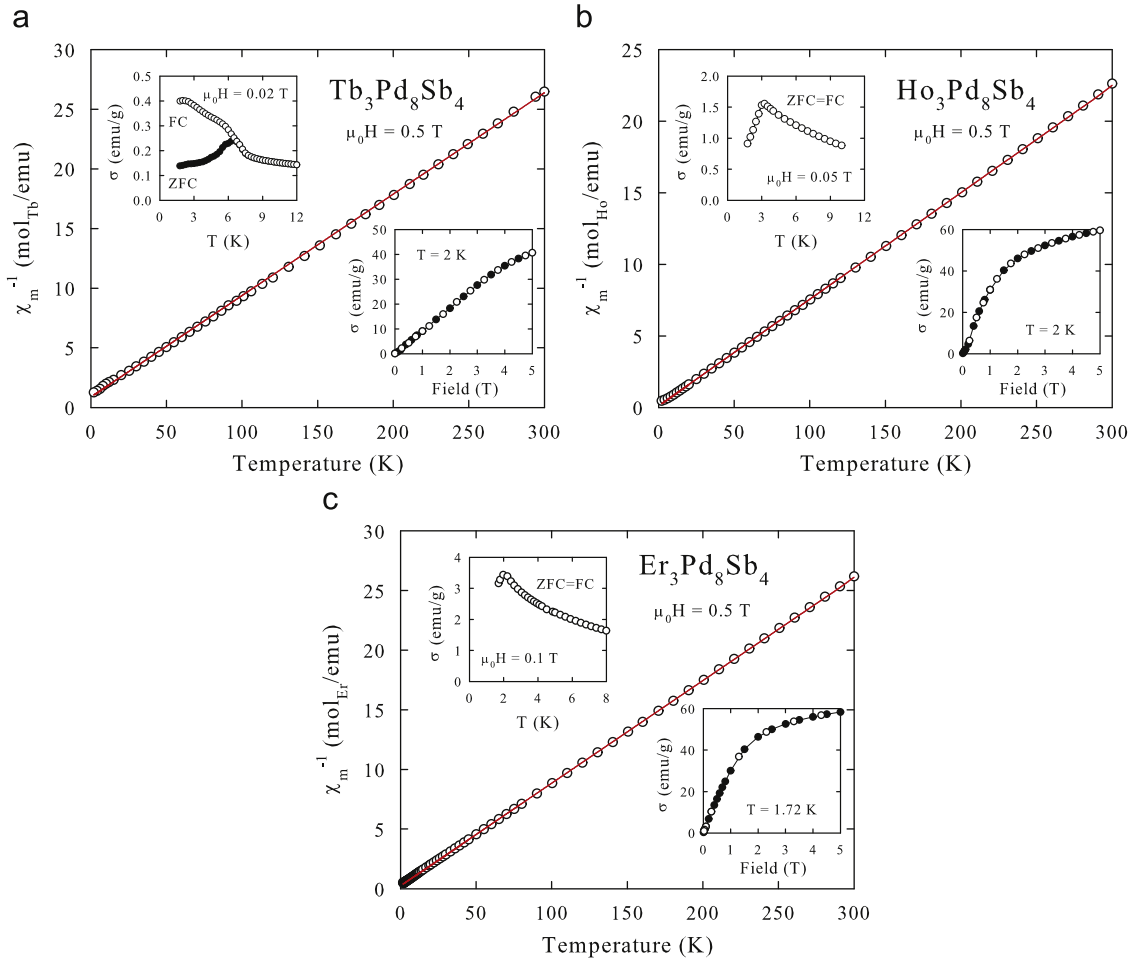

Fig. 4. Temperature dependencies of the inverse magnetic susceptibility of $Tb_3Pd_8Sb_4$ (a), $Ho_3Pd_8Sb_4$ (b) and $Er_3Pd_8Sb_4$ (c). The solid lines represent the Curie–Weiss fits discussed in the text. The upper insets show the magnetization measured at low temperatures upon cooling the samples in zero field (ZFC) and in applied field (FC). The lower insets display the field variations of the magnetization recorded at 2 K (1.72 K for $Er_3Pd_8Sb_4$) with increasing (full circles) and decreasing (open circles) field strength.

position 24*e*, and substituting the Pd atoms for the Sc atoms in the two available positions 32*f*, whereas all the Sb atoms replace the Ir atoms on their three crystallographic sites 24*d*, 4*b* and 4*a*.

Table 4 presents comparison of the crystal structure of $Er_3Pd_8Sb_4$ to the types Th_6Mn_{23} and $Mg_6Cu_{16}Si_7$ [8,9]. In these latter structures the position 4*b* is empty, but the other sites are identical to those in $Er_3Pd_8Sb_4$ and $Sc_{11}Ir_4$. As may be inferred from this table, the crystal structure of $Er_3Pd_8Sb_4$ can be considered also as a filled version of the $Mg_6Cu_{16}Si_7$-type. The Er atom is located at the Mg site, the Pd atoms replace the Cu atoms, while the Sb atoms replace the Si atoms, and moreover fill the vacancy at the 4*b* site.

Following identification of $Er_3Pd_8Sb_4$, the compounds $Ln_3Pd_8Sb_4$ (Ln=Y, Gd, Tb, Dy, Ho, Tm) have been synthesized in polycrystalline form and checked by SEM–EDS analyses and X-ray powder diffraction. The X-ray diffraction patterns indicated that the main phases are isostructural with the Er-based counterpart. The lattice parameters are listed in Table 5, including also the lattice parameter of the Er-compound refined from the X-ray powder diffraction. The lanthanide contraction is roughly respected. SEM observations of all the samples revealed large metallographic grains with atomic ratios deduced from the EDS anaylses in a good agreement with the generic formula $Ln_3Pd_8Sb_4$. In particular, no contamination of the samples by oxygen was detected. However, samples free from magnetic impurities were only achieved for Ln=Tb, Ho, Er.

3.2. Magnetic and electrical properties of the compounds $Ln_3Pd_8Sb_4$ (Ln=Tb, Ho, Er)

Fig. 3 presents the results of magnetic measurements performed on polycrystalline samples of $Tb_3Pd_8Sb_4$, $Ho_3Pd_8Sb_4$ and $Er_3Pd_8Sb_4$. For all three compounds, nearly over the entire temperature range studied, the magnetic susceptibility follows the Curie–Weiss (CW) law. The effective magnetic moments derived from the least-squares fits displayed in Fig. 3 are equal to 9.7(1), 10.37(4) and 9.64(3) μ_B per *Ln* ion, respectively. These values are in very good agreement with the values calculated within the LS coupling scheme for the respective trivalent ions (9.72 μ_B/Tb^{3+}, 10.61 μ_B/Ho^{3+} and 9.59 μ_B/Er^{3+}). The paramagnetic Weiss temperatures, derived from the CW fits are −10.2(5), −1.6(2) and −2.8(1) K, respectively. Their negative values suggest the presence of antiferromagnetic exchange interactions that eventually may result in magnetic ordering at low temperatures.

As it is apparent from the upper insets to Fig. 3, the long-range antiferromagnetic order indeed occurs in $Ho_3Pd_8Sb_4$ and $Er_3Pd_8Sb_4$ below T_N=3.0(1) and 2.0(1) K, respectively. The antiferromagnetism in the former compound is further corroborated by clear metamagnetic-like anomaly occurring in the magnetization isotherm taken in the ordered state (see the lower inset to Fig. 3b). In the case of $Er_3Pd_8Sb_4$ no such anomaly is observed (cf. the lower inset to Fig. 3c), possibly because of the closeness of the

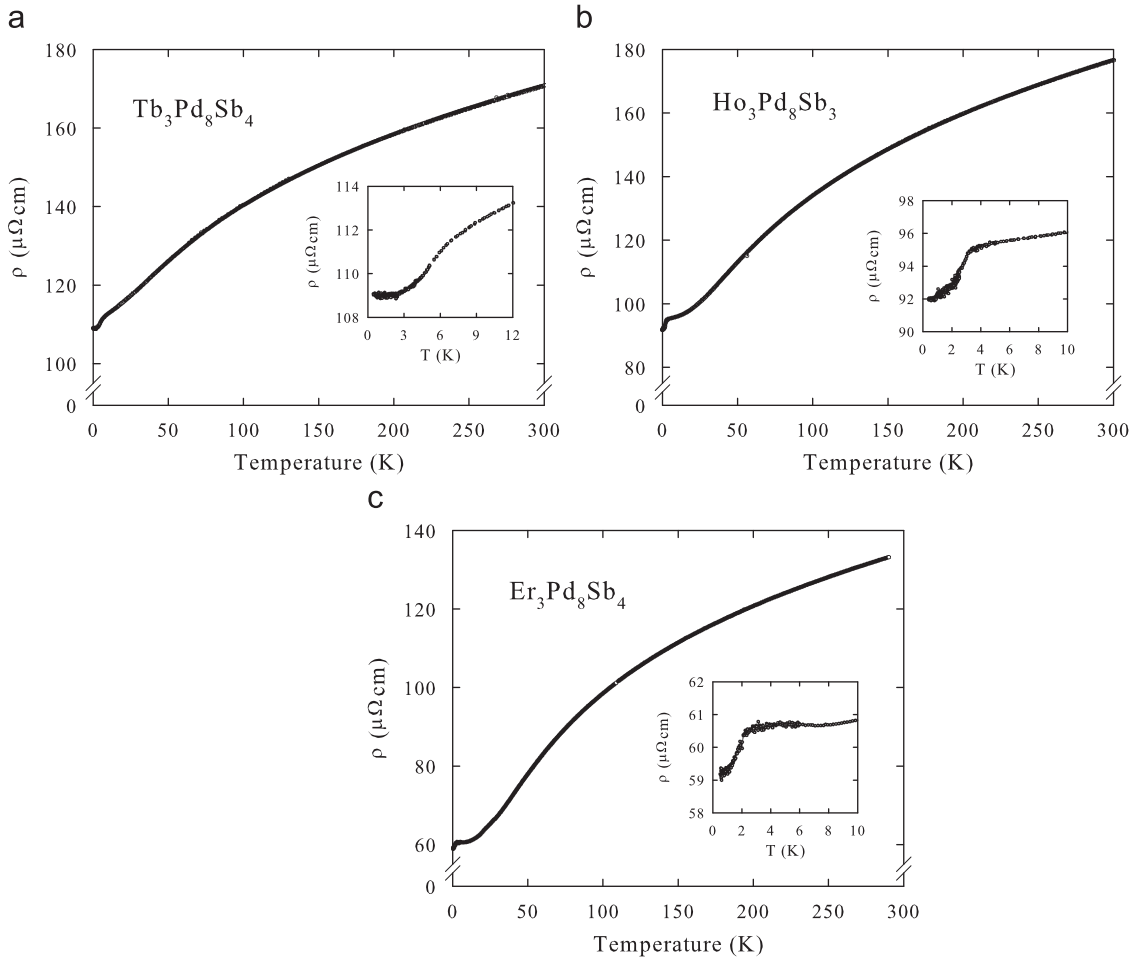

Fig. 5. Temperature dependencies of the electrical resistivity of $Tb_3Pd_8Sb_4$ (a), $Ho_3Pd_8Sb_4$ (b) and $Er_3Pd_8Sb_4$ (c). The insets zoom into the low-temperature region where the magnetic phase transitions are observed.

temperature at which the experiment was performed to the Neel point.

In contrast to the other compounds studied, the character of the ground state in $Tb_3Pd_8Sb_4$ remains rather unclear. The upper inset to Fig. 3a demonstrates clear dependence of the magnetization below 6.5 K on "magnetic history" of the specimen, namely on its cooling down to 2 K without (ZFC) or with (FC) a small applied magnetic field. The observed behavior is characteristic of systems which posses some ferromagnetic component in their magnetization, like ferromagnets, ferrimagnets, canted antiferromagnets, etc. On the other hand, the field variation of the magnetization in $Tb_3Pd_8Sb_4$ seems to contradict the ferromagnetic character. The magnetization is proportional to the field strength up to 4 T with no measurable hysteresis and negligible remanence. The hypothetical ferromagnetic ordering below $T_C=7.4(2)$ K (this value comes out from the data presented in the inset to Fig. 4a) would also be not compatible with the strongly negative paramagnetic Weiss temperature derived for the compound. For this reason one should consider a possibility that the intrinsic property of $Tb_3Pd_8Sb_4$ is actually an antiferromagnetic order that is obscured by the ferromagnetic contribution due to extremely low quantity of an unidentified impurity. Here, it is worthwhile recalling that the known terbium oxides Tb_2O_3, $TbO_{1.715}$, Tb_4O_7, $TbO_{1.823}$ and TbO_2 order magnetically below critical temperatures ranging from 2 to 8 K, but all of them are antiferromagnets [23,24].

Fig. 5 shows the temperature variations of the electrical resistivity of $Tb_3Pd_8Sb_4$, $Ho_3Pd_8Sb_4$ and $Er_3Pd_8Sb_4$. All three compounds exhibit a typical metallic behavior of lanthanide-based intermetallics with the room temperature resistivity of 130–180 μΩ cm and strongly curved $\rho(T)$ down to a kink that manifests the onset of the magnetic ordering at low temperatures. The critical temperatures derived from the resistivity data are 3.0(2) K for $Ho_3Pd_8Sb_4$ and 2.1(2) K for $Er_3Pd_8Sb_4$, in perfect agreement with T_N's obtained from the magnetic data. Interestingly, also for $Tb_3Pd_8Sb_4$ one observes a change in the slope of the resistivity curve, which occurs at about 6.5 K, i.e. close to the position of the anomaly in the magnetization. As the electrical resistivity is usually much less sensitive to magnetic impurities than magnetic susceptibility measurements, the result obtained for $Tb_3Pd_8Sb_4$ strongly supports the scenario of the intrinsic magnetic ground state in this compound.

Acknowledgments

The authors thank S. Casale and I. Péron for the investigations on the scanning electron microscope and T. Roisnel for X-ray intensity data collection at the Centre of Diffraction X (CDIFX), Rennes 1 University. This work was partially supported by the French–Polish Integrated Activity Program "POLONIUM" no. 20080PM (2008–2009).

References

[1] O.L. Sologub, P.S. Salamakha, in: K.A. Gschneidner Jr., J.-C.G. Bünzli, V.K. Pecharsky (Eds.), Handbook on the Physics and Chemistry of Rare Earths, vol. 33, 2003, pp. 35–146.
[2] R. Marazza, D. Rossi, R. Ferro, J. Less-Common Met. 75 (1980) 25–P28.
[3] S.K. Malik, D.T. Adroja, J. Magn. Magn. Mater. 102 (1991) 42–46.
[4] P. Riani, D. Mazzone, G. Zanicchi, R. Marazza, R. Ferro, Z. Metallkd. 86 (1995) 450–452.
[5] D. Kaczorowski, K. Gofryk, T. Plackowski, A. Leithe-Jasper, Yu. Grin, J. Magn. Magn. Mater. 290–291 (2005) 573–579.
[6] Yu. Mozharivskyj, H.F. Franzen, J. Solid State Chem. 152 (2000) 478–485.
[7] B. Chabot, K. Cenzual, E. Parthe, Acta Crystallogr. Sect. B36 (1980) 7–11.
[8] J.V. Florio, R.E. Rundle, A.I. Snow, Acta Crystallogr. 5 (1952) 449–457.
[9] G. Bergman, J.L.T. Waugh, Acta Crystallogr. 9 (1956) 214–457.
[10] A. Grytsiv, J.J. Ding, P. Rogl, F. Weill, B. Chevalier, J. Etourneau, C. André, F. Bourrée, H. Noel, P. Hundegger, G. Wiesinger, Intermetallics 11 (2003) 351–359.
[11] X.-A. Chen, W. Jeitschko, M.H. Gerdes, J. Alloys Compd. 234 (1996) 12–18.
[12] D. Berthebaud, O. Tougait, M. Potel, E.B. Lopes, A.P. Gonçalves, H. Noel., J. Solid State Chem. 180 (2007) 2926–2932.
[13] A. Grytsiv, X.-Q. Chen, P. Rogl, R. Podloucky, H. Schmidt, G. Giester, V. Pomjakushin, J. Solid State Commun. 40 (1981) 1015–1018.
[14] W. Krause, G. Nolze, Federal Institute for Materials Research and Testing, Berlin, Germany.
[15] Bruker-AXS, in: Collect, Denzo, Scalepack, Sortav, Kappa CCD Program Package, Nonius BV, Delft, The Netherlands, 1998.
[16] R.H. Blessing, Acta Crystallogr. Sect. A 51 (1995) 33–38.
[17] A. Altomare, M.C. Burla, M. Camalli, G.L. Cascarano, C. Giacovazzo, A. Guagliardi, A.G.G. Moliterni, G. Polidori, R.J. Spagna, J. Appl. Crystallogr. 32 (1999) 115–119.
[18] L.G. Akselrud, Yu. N. Grin, V.K. Pecharsky, P. Yu.Zavalji, CSD97-Universal program package for single crystal and powder data treatment, version no. 7, 1997.
[19] L.M. Gelato, E. Parthé, STRUCTURE TIDY—a computer program to standardize crystal structure data, J. Appl. Crystallogr. 20 (1987) 139–143.
[20] G. Bergerhoff,DIAMOND, Gerhard—DomagkStraβ 1, 53121 Bonn, Germany, 1996.
[21] P.I. Kripiakevich, in: Structure Types of the Intermetallic Compounds, Nauka, Moscow, 1977 (in Russian).
[22] I. Ye., O.I.Bodak Gladyshevskyy, in: The Crystal Chemistry of Intermetallic Compounds of Rare-earth Metals, Vyshcha Shkola, Lvov, 1982 (in Russian).
[23] R.W. Hill, J. Phys. C: Solid State Phys. 19 (1986) 673–682.
[24] G. Adachi, N. Imanaka, Z.C. Kang (Eds.), Binary Rare Earth Oxides, Kluwer Academis Publishers, 2004.